TECHNICAL REPORT
NATICK/TR-92/019

AD A 245 069

FINITE ELEMENT MODELING OF FRAGMENT PENETRATION OF THIN STRUCTURAL COMPOSITE LAMINATES

By
Andreas M. Blanas

December 1991

Final Report
October 1988 - September 1991

UNITED STATES ARMY NATICK
RESEARCH, DEVELOPMENT AND ENGINEERING CENTER
NATICK, MASSACHUSETTS 01760-5000

AERO-MECHANICAL ENGINEERING DIRECTORATE

DISCLAIMERS

The findings contained in this report are not to be construed as an official Department of the Army position unless so designated by other authorized documents.

Citation of trade names in this report does not constitute an official endorsement or approval of the use of such items.

DESTRUCTION NOTICE

For Classified Documents:

Follow the procedures in DoD 5200.22-M, Industrial Security Manual, Section II-19 or DoD 5200.1-R, Information Security Program Regulation, Chapter IX.

For Unclassified/Limited Distribution Documents:

Destroy by any method that prevents disclosure of contents or reconstruction of the document.

DISCLAIMER NOTICE

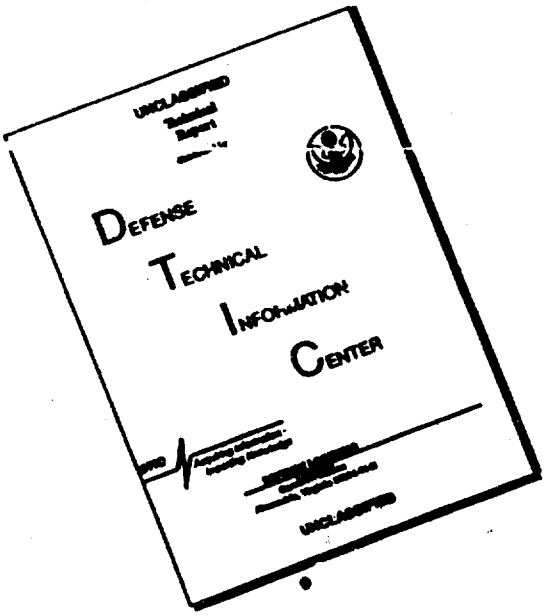

THIS DOCUMENT IS BEST QUALITY AVAILABLE. THE COPY FURNISHED TO DTIC CONTAINED A SIGNIFICANT NUMBER OF PAGES WHICH DO NOT REPRODUCE LEGIBLY.

REPORT DOCUMENTATION PAGE

Form Approved
OMB No. 0704-0188

1. AGENCY USE ONLY (Leave blank)	2. REPORT DATE	3. REPORT TYPE AND DATES COVERED
	December 1991	Final Report Oct 88 - Sep 91

4. TITLE AND SUBTITLE

Finite Element Modeling of Fragment Penetration of Thin Structural Composite Laminates

5. FUNDING NUMBERS

P.E.: 61102A
P.N.: 1L161102AH52
T.A.: 02
W.U.: 041
AGG CODE: T/B1286

6. AUTHOR(S)

Andreas M. Blanas

7. PERFORMING ORGANIZATION NAME(S) AND ADDRESS(ES)

U.S. Army Natick Research, Development and Engineering Center
Kansas Street
Natick, MA 01760-5017

8. PERFORMING ORGANIZATION REPORT NUMBER

NATICK/TR-92/019

9. SPONSORING/MONITORING AGENCY NAME(S) AND ADDRESS(ES)

10. SPONSORING/MONITORING AGENCY REPORT NUMBER

11. SUPPLEMENTARY NOTES

12a. DISTRIBUTION/AVAILABILITY STATEMENT

Approved for public release; distribution unlimited.

12b. DISTRIBUTION CODE

13. ABSTRACT *(Maximum 200 words)*

Fiber-reinforced composite laminates are increasingly used in tactical shelters for structural and ballistic resistance purposes to provide survivability in the field. The development of an analytical technique to predict the level of ballistic protection provided by composite laminates would greatly enhance the effective use of new materials and composite design concepts and reduce the need for testing.

The first stage of the effort involves using the finite element code DYNA3D to macromechanically model the impact, and possible penetration, of a composite shelter wall by fragments from conventional bomb bursts. The model accommodates fragments of different material, shape, grain size and velocity, and composite walls of different material, ply orientation, areal density and volume fractions.

Input models for fragments and composite laminates, having layup and material configuration similar to experimental models, have been run. Plots of ballistic limit versus areal density for different materials and fragment grain sizes have been obtained and compared with experimental results. Parametric studies, measuring the effects of varying input model's material properties on the ballistic limit, have also been conducted.

14. SUBJECT TERMS			15. NUMBER OF PAGES
FINITE ELEMENT MODELING	TACTICAL SHELTERS	FRAGMENTS	54
FRAGMENT PENETRATION	SHELTERS	MODELS	16. PRICE CODE
COMPOSITE LAMINATES	FIBER-REINFORCED COMPOSITES		
	BALLISTIC RESISTANCE		

17. SECURITY CLASSIFICATION OF REPORT	18. SECURITY CLASSIFICATION OF THIS PAGE	19. SECURITY CLASSIFICATION OF ABSTRACT	20. LIMITATION OF ABSTRACT
Unclassified	Unclassified	Unclassified	UL

Contents

Figures

Tables

Preface

The work reported herein was performed under project number 1L161102AH5202041, Analytical Modeling of Ballistic Penetration of Composite Laminates, from October 1, 1988 to September 30, 1991.

The author wishes to acknowledge the generosity of Jo Anne Levatin and J. O. Hallquist of the Lawrence Livermore National Laboratory, Livermore, California, who supplied the source computer codes used in this project. Also acknowledged is Frank S. Hodi of the Materials Dynamics Branch, Materials Technology Laboratory, for his valuable experimental work. Finally, a note of appreciation to John Calligeros of the Engineering Technology Division, Aero-Mechanical Engineering Directorate, Natick, for his direction and assistance provided during the program.

The following are registered trade names: Kevlar-29, 3M Co., Scotchply, Owens Corning Fiberglass (OCF), Du Pont Co., Lewcott Co., MATLAB, SUN Computer Microsystems, Stardent Computer. Citation of trade names in this report does not constitute an official endorsement or approval of use of such items.

Finite Element Modeling of Fragment Penetration of Thin Structural Composite Laminates

Introduction

Composite materials have been used as engineering materials for structural support and ballistic protection because of their high strength to weight ratios and effective ballistic performance. Even though analytical techniques for the response of composite materials under various loads have been developed, no comparable analytical methods of modeling the ballistic impact and penetration of composite laminates are available.

Traditionally, work has concentrated on penetration and prediction of ballistic limits for metals, such as steel and aluminum, and the development thereof of hydrocodes to model the penetration process of those materials. Only empirical or semiempirical models using curvefitting techniques have been used to provide design charts for composite structures and their ballistic resistances based on experiment. However, reliance solely on experimental methods could become expensive and certainly limit the possibilities of a near-optimum design if the number of variables involved are taken into consideration.

A general description of the problem considered here is shown in Fig. 1 [1]. A fragment from a conventional bomb burst impacts a composite material target wall at a moderate velocity of 500 to 2500 feet per second. The size and shape of the fragment and the material, ply orientation and areal density of the target can vary. For modeling purposes, steel fragment simulating projectiles (FSP, MIL-P-46593A) of three mass levels, 5.85-, 17- and 44- grains, are used. Composite laminates such as Owens Corning Fiberglass (R) panels, 3M Scotchply 1002 (R) panels and Kevlar-29 (R) reinforced plastic panels having typical material properties and variable areal densities (1.0 to 2.50 pounds per square foot) are considered in an effort to reproduce the experiment [2].

Hydrocode DYNA3D [3a] is used to model the problem. DYNA3D is a finite element computer code for analyzing the large deformation present during fragment penetration. A mesh generator is used to create the input model's geometry. A postprocessor is used to interpret and graphically display results. The graphics package of MATLAB [4] is also used to plot ballistic limits versus areal densities.

Figure 1. A General Description of the Impact Problem [1].

Even though ballistic penetration is a localized problem around the area of impact, a decision was made to look at the macromechanical method of analysis first. This method is traditionally used for structural analysis of composite laminates. This first stage of the analysis allows us to quickly study and qualitatively compare the macromechanically obtained analytical results with the experiment. Some parametric studies also were conducted, in an effort to measure the effect of varying material properties on the ballistic limit and penetration process.

Approach

Macromechanics vs. Micromechanics

Composite materials, unlike most common engineering materials (e.g., steel, aluminum), are heterogeneous and anisotropic. A heterogeneous body has nonuniform properties and therefore they are a function of position in the body. An anisotropic body has material properties that are different in all directions or they are a function of orientation at a point in the body. Because of the inherent heterogeneous nature of composite materials, they can be studied from two points of view: micromechanics and macromechanics. The border line between these two approaches has been a subject of ambiguity among composite materials analysts, and numerous definitions have been established depending on the nature and scope of the analysis.

In the context of this paper, we will refer to macromechanics as being the study of composite material laminates behavior wherein each ply is presumed homogeneous and the constituent materials are detected only as averaged apparent properties of the lamina. On the other hand, we will refer to micromechanics as being the study of composite material behavior wherein the interaction of the constituent materials (fibers and resin) is examined on a localized microscopic scale [5].

Experimental Data Acquisition - Materials

Experimental investigations were conducted to determine the fragment ballistic resistance and damage tolerance of different composite laminates and to evaluate composite materials that might be useful for armor on tactical shelters. Experimental results, such as ballistic limits (V50) vs. areal densities [2], [6] are used for comparison purposes with analytically obtained results.

Ballistic limit (V50) is the velocity calculated as the average of six test velocities within a spread or velocity interval of 125 feet per second, half of which result in complete penetration of the target and half of which result in incomplete or partial penetration of the target. A complete penetration of the target is defined as an impact that results in a hole in a witness sheet made of a 0.020 inch-thick aluminum plate parallel to and six inches behind the target [2]. The ballistic performance of a composite target wall is significantly affected by the properties and volume fractions of the constituent materials (fiber, resin), ply orientation, stacking sequence of the layup and the thickness of the wall (areal density).

Among a number of materials tested, the following are some that were also used as a base for comparison with analytical results [2]:

1. Owens Corning Fiberglass (OCF) Structural Panels. Woven S-2 glass and a typical resin type, content, sizing, and cure cycle at 220 degrees F.
2. 3M Scotchply Panels, Type 1002 - Nonwoven E-Glass continuous filament, reinforced epoxy resin laminates - crossply orientation.
3. Kevlar-29 Reinforced Plastic Panels - Reinforcement made up of 16 oz/sq yd fabric of 3000-denier yarn woven into 4 by 4 basket weave count 21 by 21 per inch. Resin is a preimpregnated polyester flame retardant resin, supplied by Lewcott Co. (LC-357 FR).

Code Search and Code Structure

Two-dimensional numerical simulations of impact and penetration phenomena have been performed since the early seventies. In recent years, interest has arisen in three dimensional codes. These codes were developed to solve impact problems characterized by [1]:

- localized material response as contrasted to global structural response
- shock wave problems characterized by steep stress or high velocity gradients
- time of loading and response in the milli or microsecond regime.

Originally, our intention was to develop our own in-house computer code. Nevertheless, a hydrocode search revealed that this development would be an enormous task. Further research showed that a code using a macromechanical model existed. A three-dimensional finite element code, called DYNA3D [3a], was obtained from Lawrence Livermore National Lab (LLNL). This code has a composite damage material model [7]. A graphics package, containing a preprocessor (INGRID [8]) and a postprocessor (TAURUS [9]), was also obtained from LLNL. All of the above software is free of charge, well-documented and runs on both our SUN microsystem and Stardent minisuper computers. Source files of all the above codes were obtained, allowing the user to define a new material model, if needed, and recompile the code.

A generic structure of the computational process followed by these codes is shown in Fig. 2 [1]. A preprocessor is used to generate the finite element mesh and define the material properties of the model. Initial and boundary conditions and material interfaces are also defined. The main code uses a finite element technique to discretize the conservation equations as coupled to the material model equations. These equations are then integrated in time. Finally a postprocessor is used to interpret and graphically display results, such as deformation modes, stress and strain fields and velocities.

THE COMPUTATIONAL PROCESS

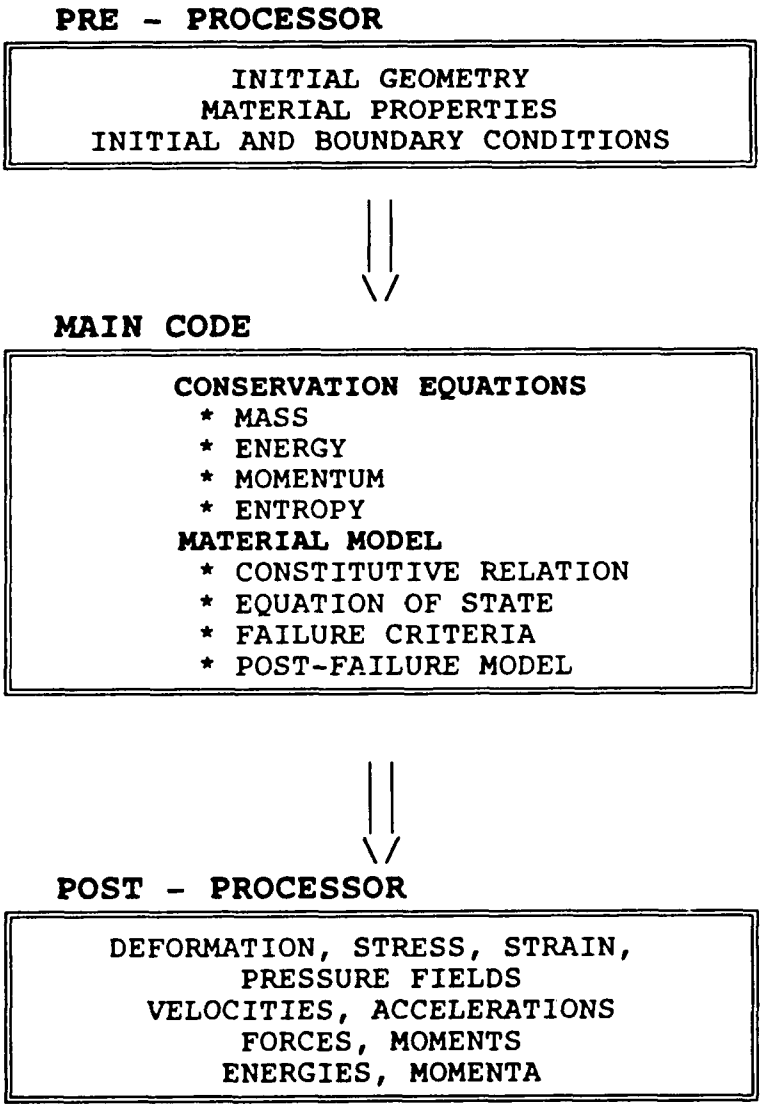

Figure 2. Structure of the Computational Process [1].

The most important aspect of the main program is the material model equations. Appropriate use of the constitutive relations, failure criteria and postfailure model is essential to the modeling of the material behavior. Quasistatic failure models may be proven inadequate in situations involving dynamic and high-rate loadings.

DYNA3D

DYNA3D [3c] is an explicit three-dimensional finite element code for analyzing the large deformation dynamic response of solids and structures. It is a Langrangian code and it follows the motion of fixed elements of mass. The computational grid is fixed in the material and distorts with it. Equations of motion are integrated in time explicitly using the central difference method. DYNA3D contains 28 material models and eleven equations of state. Spatial discretization is achieved by the use of the following elements: 8 node solid hexahedron, 2 node beam, 4 node shell, 8 node solid shell, triangular shell and rigid bodies.

An artificial viscosity is used to treat shock wave development and propagation. Shocks result from the phenomena that sound speed increases with increasing pressure. A pressure wave gradually steepens until it propagates as a discontinuous disturbance called shock. Shocks lead to jumps in pressure, density, particle velocity and energy. The artificial viscosity method eliminates shock discontinuities by smearing the shock fronts over a small number of elements.

DYNA3D has an extensive slide-line capability. Sliding interfaces are used where continuity of normal stress and velocity components between two surfaces is required. They are also used to provide movement of interface nodes between two surfaces that are expected to slide on each other (penetration of projectiles into materials).

Langrangian calculations lose accuracy as the mesh distorts. In explicit calculations used by DYNA3D, the time step size will drop resulting in very high cost. A rezoning capability exists. The user can interrupt the calculation, view the calculation, including the display of all history variables, decide whether to modify the mesh and do so if necessary; all without stopping the calculation.

Governing Equations

The conservation equations used by DYNA3D [5b] are shown here. Consider the body shown in Fig. 3.

We are seeking a solution to the momentum equation

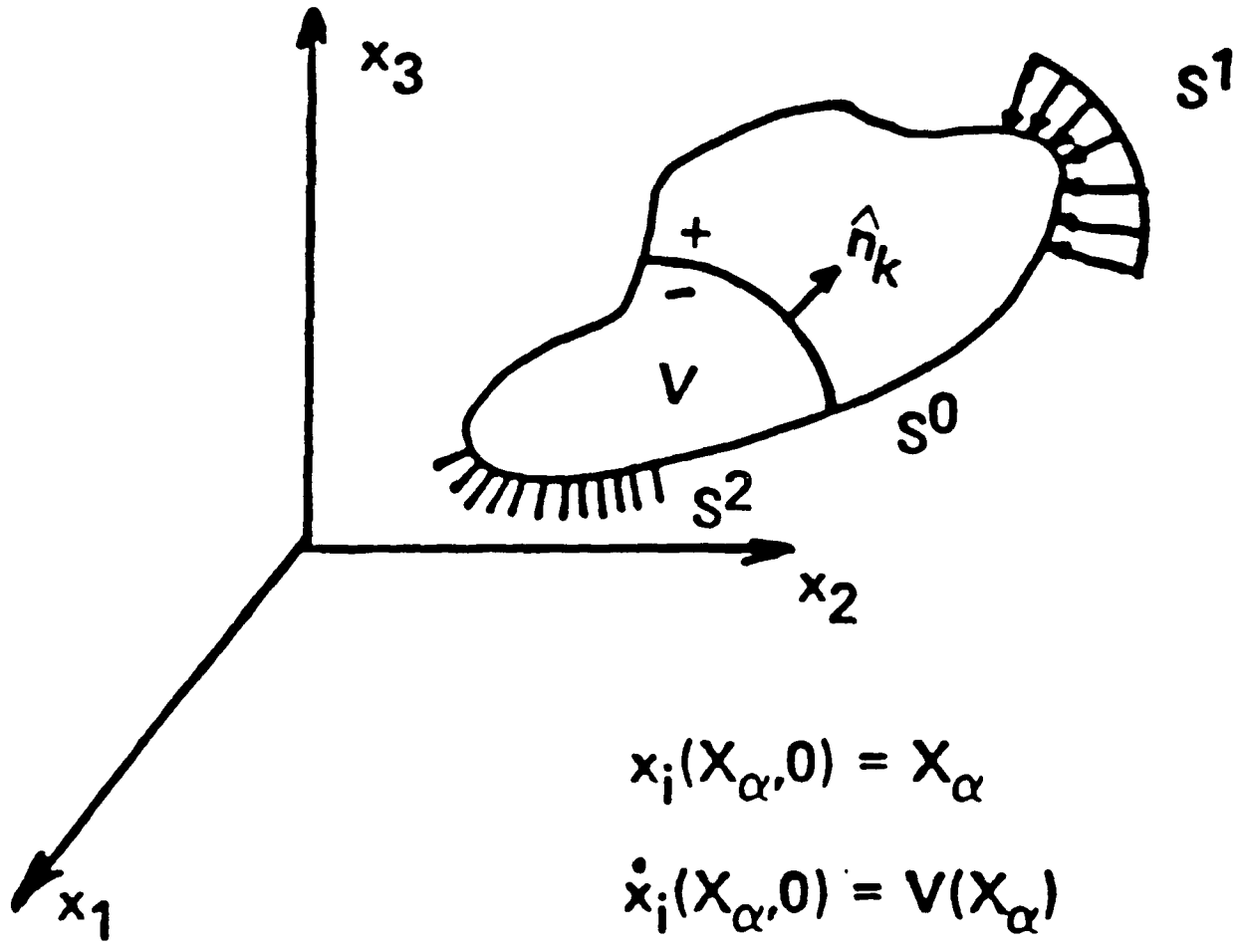

Figure 3. A Body in a Fixed Rectangular Cartesian Coordinate System, Lagrangian Formulation Considered [3b].

$$\sigma_{ij,j} + \rho b_i = \rho \ddot{x}_i \qquad (1)$$

satisfying the traction boundary conditions,

$$\sigma_{ij} n_j = S_i(t) \qquad on \ S^1,$$

the displacement boundary conditions,

$$x_i(X_a, t) = K_i(t) \qquad on \ S^2,$$

and the contact discontinuity

$$(\sigma_{ij}^{+} - \sigma_{ij}^{-}) n_j = 0 \qquad on \ S^0.$$

Here σ is the Cauchy stress, ρ is the current mass density, b_i is the body force, $\ddot{x}_i$ is the acceleration, the comma denotes covariant differentiation, and n_j is a unit outward normal to a boundary element.

The mass conservation equation is

$$\rho J = \rho_o \qquad (2)$$

where J is the determinate of the deformation gradient matrix, and ρ_o is the reference density.

The energy equation is stated as

$$\dot{E} = V s_{ij} \dot{e}_{ij} - (p + q) \dot{V} \qquad (3)$$

where s_{ij} and p are the deviatory stresses and pressure, $\dot{e}_{ij}$ is the strain rate tensor and V is relative volume.

The equation for total stress is

$$\sigma_{ij} = s_{ij} - (p + q) \delta_{ij} \qquad (4)$$

where q is the bulk viscosity and δ_{ij} is the Kronecker delta.

We can write a weak form of the equilibrium equation as [3c]

$$\int(\rho\ddot{x} - \sigma_{ij,j} - \rho b_i)\delta x_i dv + \int(\sigma_{ij}n_j - S_i)\delta x_i ds + \int(\sigma_{ij}^{+} - \sigma_{ij}^{-})n_j\delta x_i ds = 0 \quad (5)$$

Application of the divergence theorem leads to

$$\delta\pi = \int\rho\ddot{x}_i\delta x_i dv + \int\sigma_{ij}\delta x_{i,j}dv - \int\rho b_i\delta x_i dv - \int S_i\delta x_i ds = 0 \quad (6)$$

which is a statement of the principle of virtual work. This last equation can be discretized and solved by using a finite element method as shown in reference [3c]. The central difference method is used to explicitly integrate in time.

Composite Damage Material Model

Failure criteria proposed by [7] are used here. Chang and Chang use similar equations (equilibrium, total stress) as DYNA3D to do stress analysis. In addition, [7] use classical lamination theory to form the reduced moduli and check for failure in each ply through the thickness. Plane stress condition is assumed and three different inplane failure modes are looked at: matrix cracking, fiber-matrix shearing and fiber breakage. DYNA3D uses the same failure criteria for each element since the one point integration is used for the 8 node hexahedron solid element.

The matrix failure criterion is

$$\left(\frac{\sigma_y}{Y_t}\right)^2 + \frac{\dfrac{\sigma_{xy}^2}{2G_{xy}} + \dfrac{3}{4}\alpha\sigma_{xy}^4}{\dfrac{S_c^2}{2G_{xy}} + \dfrac{3}{4}\alpha S_c^4} = e_m^2 \quad (7)$$

σ_y and σ_{xy} are the transverse and shear stresses in each ply, G_{xy} is the initial ply shear modulus, Y_t is the transverse tensile strength and S_c is the in-situ ply shear strength measured from a cross-ply laminate, $[0/90]_s$, with the same thickness as the laminate considered.

For laminates with linear elastic behavior, $\alpha = 0$, and the criterion reduces to

$$\left(\frac{\sigma_y}{Y_t}\right)^2 + \left(\frac{\sigma_{xy}}{S_c}\right)^2 = e_m^2 \tag{8}$$

For the above equations, matrix cracking occurs if $e_m \geq 1$.

Compressive failure in matrix is predicted by the Hashin failure criterion

$$\left(\frac{\sigma_y}{2S_c}\right)^2 + \left[\left(\frac{Y_c}{2S_c}\right)^2 - 1\right]\frac{\sigma_y}{Y_c} + \frac{\frac{\sigma_{xy}^2}{2G_{xy}} + \frac{3}{4}\alpha\sigma_{xy}^4}{\frac{S_c^2}{2G_{xy}} + \frac{3}{4}\alpha S_c^4} = e_d^2 \tag{9}$$

Here Y_c is the transverse compressive strength of a unidirectional ply.

For linear elastic laminates eq. (9) reduces to

$$\left(\frac{\sigma_y}{2S_c}\right)^2 + \left[\left(\frac{Y_c}{2S_c}\right)^2 - 1\right]\frac{\sigma_y}{Y_c} + \left(\frac{\sigma_{xy}}{S_c}\right)^2 = e_d^2 \tag{10}$$

Matrix compression failure occurs, in a layer or an element, if $e_d \geq 1$.

Both fiber-matrix shearing and fiber breakage are predicted by

$$\left(\frac{\sigma_x}{X_t}\right)^2 + \frac{\frac{\sigma_{xy}^2}{2G_{xy}} + \frac{3}{4}\alpha\sigma_{xy}^4}{\frac{S_c^2}{2G_{xy}} + \frac{3}{4}\alpha S_c^4} = e_f^2 \tag{11}$$

Here σ_x and X_t are the longitudinal tensile stress and strength in each ply.

For linear elastic laminates the criterion reduces to

$$(\frac{\sigma_x}{X_t})^2 + (\frac{\sigma_{xy}}{S_c})^2 = e_f^2 \qquad (12)$$

The fiber failure criterion states that when, in any one of the plies or elements in a laminate, the combined stresses σ_x and σ_{xy} satisfy the criterion ($e_f \geq 1$), that element fails by either fiber breakage or fiber-matrix shearing.

Description of DYNA3D Model Used

The geometry of the three-dimensional model used is shown in Fig. 4. A kinematic/isotropic elastic-plastic material model was used for modeling the fragment simulating projectile. The composite damage material model [7] was used to model the composite wall. An 8 node solid hexahedron element was employed to model both the fragment and the composite target meshes. Half symmetry was used to reduce calculation time. Symmetry boundary conditions were set along the y=0 plane. A fixed-boundary condition was imposed along the outer edge of the target. A coarse geometric mesh was constructed at the outer part of the wall away from the point of impact. A finer mesh is required near the impact zone because of the high rates of stress change and large deformations developed.

The model accommodates fragments with varying shape, grain size, material and initial velocities. The composite wall model could also have varying material and volume fractions, ply orientation and thickness. Material properties for OCF Fiberglass, Scotchply 1002 and Kevlar-29 panels are listed in Appendix A.

kevlar 1/2 sym. 44grn .24"
time = 0.00000E+00

Half Symmetry

||
\/ **V is Fragment Initial Velocity**

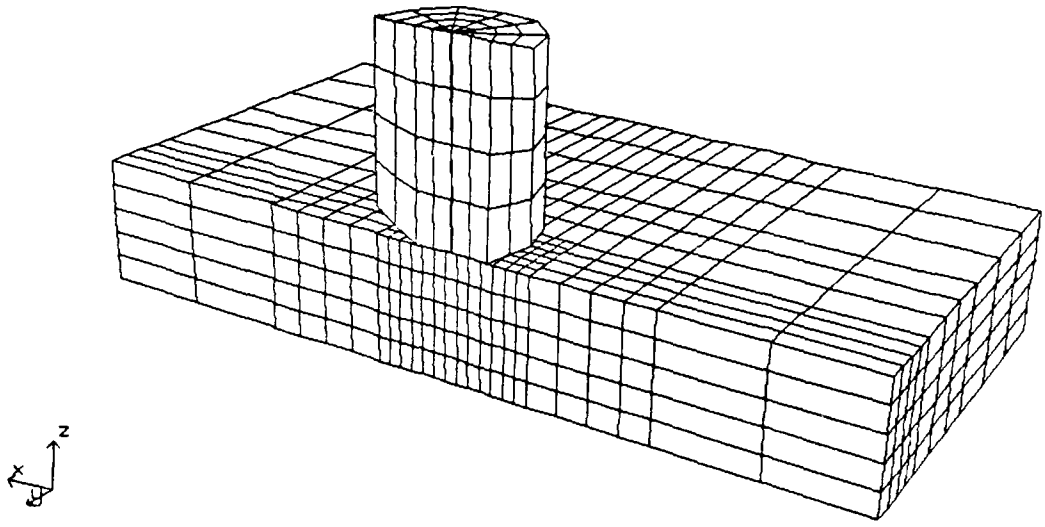

MODEL ACCOMMODATES:
- Fragments with varying: Shape, Grain Size, Material, Initial Velocity.
- Target wall with varying: Material, Ply Orientation, Thickness and Volume Fractions.

Figure 4. Geometry Mesh of DYNA3D Model used.

Results and Comparison to Experiment

Several cases of variable wall thickness (three different thicknesses per material) were considered in an effort to match the areal densities used in the experiment. Again, among a number of materials tested, the following three materials were analytically modeled and compared to experiment:

1. Owens Corning Fiberglass (OCF) Structural Panels. Woven S-2 glass and a typical resin type, content, sizing, and cure cycle at 220 degrees F.
2. 3M Scotchply Panels, Type 1002 - Nonwoven E-Glass continuous filament, reinforced epoxy resin laminates - crossply orientation.
3. Kevlar-29 Reinforced Plastic Panels - Reinforcement made up of 16 oz/sq yard fabric of 3000-denier yarn woven into 4x4 basket weave count 21x21 per inch. Resin is a preimpregnated polyester flame-retardant resin, supplied by Lewcott Co. (LC-357 FR).

Typical properties of the above materials are shown in Appendix A. Steel fragment simulating projectiles of three mass levels 5.85, 17 and 44 grains impacting the wall were considered for each wall thickness. The dimensions and shape of each projectile were taken from MIL-P-46593A. Typical steel projectile material properties were used (Appendix A).

In all, 27 different configurations of varying either material, wall thickness or projectile weight were modeled. Table 1 shows all the cases modeled. A typical case of a 0.24 inch-thick Kevlar wall in the process of penetration by a 44 grain fragment is shown in Fig. 5. Both the undeformed mesh prior to impact and the deformed mesh at a time of 21.9 microseconds after impact are shown.

Table 1. Twenty Seven Cases were modeled.

Fragment Size	Materials Used								
	Gl/Ep. 3M Scotchply			S-2 Gl/Pol. OCF			Kv-29/Pol. Dupont		
	Areal Density (psf)			Areal Density (psf)			Areal Density(psf)		
(Grains)	1.38	1.84	2.40	1.37	1.99	2.36	1.01	1.45	1.75
5.85	X	X	X	X	X	X	X	X	X
17.0	X	X	X	X	X	X	X	X	X
44.0	X	X	X	X	X	X	X	X	X

kevlar 1/2 sym. 44grn .24"

0.24" Thick Wall
Woven Kv-29/Polyester
44 Grain FSP

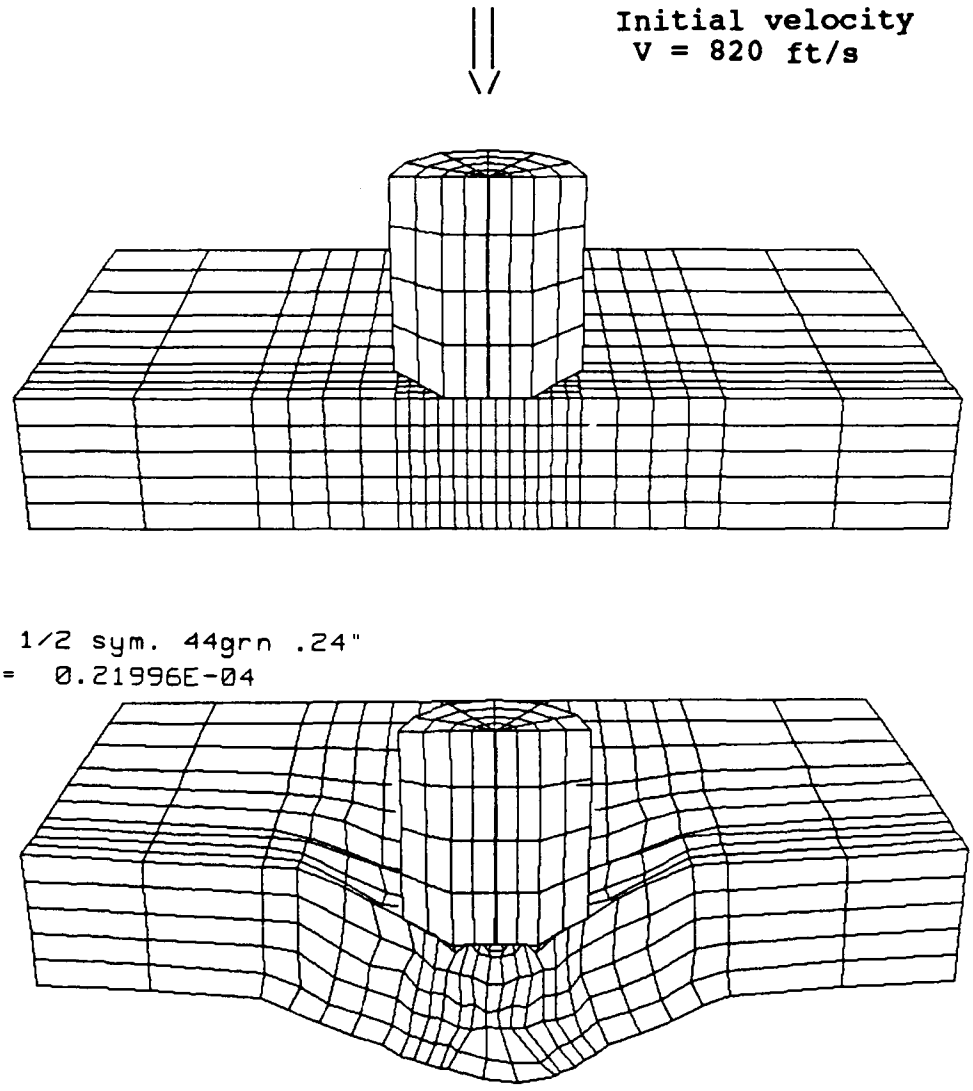

Figure 5. Kevlar 29 Wall Prior to and During Penetration.

Stress contours and contour values of the fragment and the wall showing Von-Mises effective stress are shown in Fig. 6. Note the high stress concentration contours at the localized area around the projectile impact. Failure occurs at each element if the stress levels exceed the strength values. Failed elements cannot carry any further tensile or shear loads but will carry, when reloaded, compressive hydrostatic stresses.

In addition to effective stress contours, effective strain contours for both the projectile and the wall are shown in Fig. 7. Again, it can be noted that the highest strains occur around the localized impact area. Failure criteria could have been based on volumetric strains but since the strains at failure for the materials used are not known, modeling of failure was limited to the stress failure approach. One of the advantages of analytical modeling over experimental methods is the ability of predicting the stress and strain contours of the material at any time during penetration. Knowledge of the strain rates during impact is an important aspect of modeling if, at a later time, constitutive material modeling at high strain rates is desired. At such model, the material properties would have to be updated as a function of dynamic strain rates in time. Presently, a lack of knowledge of high strain rate properties of most composite materials prohibits the successful development of such a model.

A ballistic limit was approximated as the initial velocity of the fragment carrying enough kinetic energy to completely penetrate the wall. An iterative trial and error process was used in order to approximate the ballistic limit for each of the 27 cases run. An initial velocity was guessed and used as input velocity. Results of deformation of the wall and the fragment penetrating it were carefully inspected visually. If residual velocities of the fragment were close to zero, or small, compared to the striking velocities, the initial velocity of the fragment was then considered to be the ballistic limit V50. If penetration did not occur as determined by visual inspection or if the residual velocity of the fragment was not small, a new initial fragment velocity was input. This iteration procedure was then repeated until a suitable ballistic limit was determined. An average of five to six runs per case were run. Detailed results for each material, as compared to the experiment, are shown in Tables 2,3,4.

kevlar 1/2 sym. 44grn .24"
time = 0.21996E-04
contours of eff. stress (v-m)
min= 0.142E+05 in element 81
max= 0.111E+06 in element 10

PSI

contour values
A= 2.23E+04
B= 3.24E+04
C= 4.25E+04
D= 5.25E+04
E= 6.26E+04
F= 7.27E+04
G= 8.27E+04
H= 9.28E+04
I= 1.03E+05

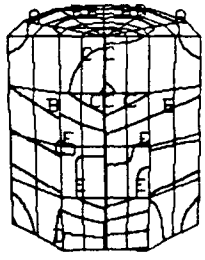

kevlar 1/2 sym. 44grn .24"
time = 0.21996E-04
contours of eff. stress (v-m)
min= 0.000E+00 in element 1082
max= 0.311E+06 in element 142

PSI

contour values
A= 2.62E+04
B= 5.86E+04
C= 9.09E+04
D= 1.23E+05
E= 1.56E+05
F= 1.88E+05
G= 2.20E+05
H= 2.53E+05
I= 2.85E+05

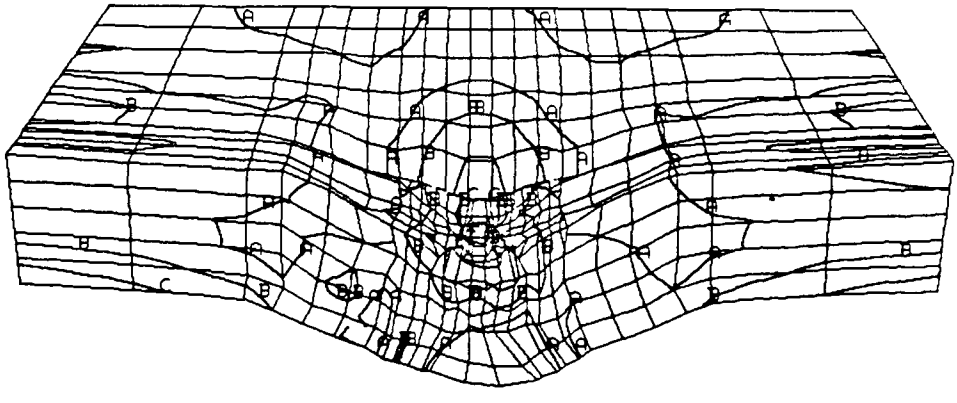

Figure 6. Von Mises Effective Stress Contours.

mIN/IN

kevlar 1/2 sym. 44grn .24"
time = 0.21996E-04
contours of eff. plastic strain
min= 0.000E+00 in element 96
max= 0.210E-01 in element 83

contour values
A= 1.76E-03
B= 3.94E-03
C= 6.12E-03
D= 8.31E-03
E= 1.05E-02
F= 1.27E-02
G= 1.49E-02
H= 1.70E-02
I= 1.92E-02

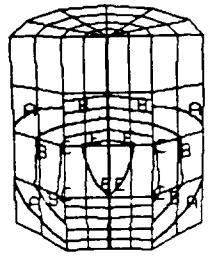

mIN/IN

kevlar 1/2 sym. 44grn .24"
time = 0.21996E-04
contours of eff. plastic strain
min= 0.000E+00 in element 1219
max= 0.100E+01 in element 1296

contour values
A= 8.40E-02
B= 1.88E-01
C= 2.92E-01
D= 3.96E-01
E= 5.00E-01
F= 6.04E-01
G= 7.08E-01
H= 8.12E-01
I= 9.16E-01

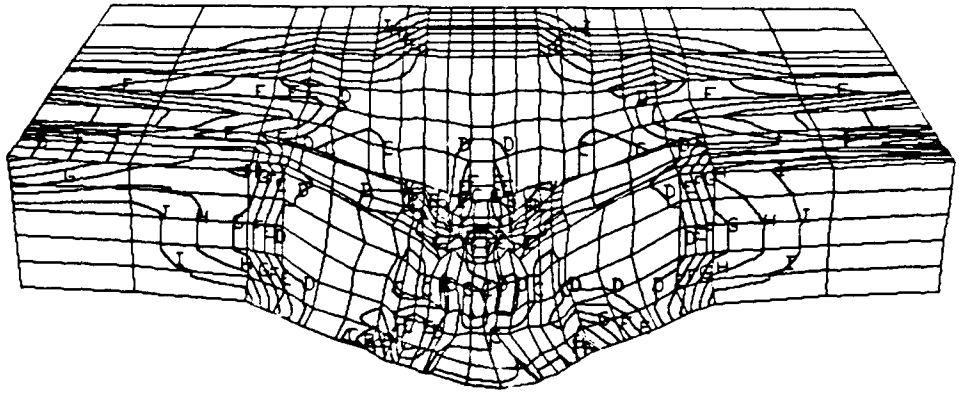

Figure 7. Effective Strain Contours.

Table 2. Comparison of Ballistic Data for S-2 Glass.

Areal Density (psf)	Thick-ness (inch)	BALLISTIC LIMIT (V50) - (ft/sec)					
		Experiment			DYNA3D		
		5.85 gr	17 gr	44 gr	5.85 gr	17 gr	44 gr
1.37	.14	1447	1096	916	1541	791	460
1.99	.20	1997	1461	1053	2750	1458	710
2.36	.24	2121	1634	1233	2900	2290	1040

Table 3. Comparison of Ballistic Data for 3M Scotchply.

Areal Density (psf)	Thick-ness (inch)	BALLISTIC LIMIT (V50) - (ft/sec)					
		Experiment			DYNA3D		
		5.85 gr	17 gr	44 gr	5.85 gr	17 gr	44 gr
1.38	.15	1448	1037	646	1500	735	460
1.84	.20	1752	1240	966	2500	1125	670
2.40	.26	2039	1540	1149	2900	2330	960

Table 4. Comparison of Ballistic Data for Kevlar 29.

Areal Density (psf)	Thick-ness (inch)	BALLISTIC LIMIT (V50) - (ft/sec)					
		Experiment			DYNA3D		
		5.85 gr	17 gr	44 gr	5.85 gr	17 gr	44 gr
1.01	.120	1519	1255	1095	1085	585	375
1.45	.199	1645 2161 1901	1549	1342	2166	1085	625
1.75	.243	1941	1591	1366	2666	1625	820

Graphical representation of comparisons between DYNA3D analytical results and experiment are also shown in Figures 8 to 13. In these figures, the ballistic limit V50 (ft/s) for a specific projectile grain size is plotted versus the areal density (lbs/ft^2) for each material. The plotting package of MATLAB is used to fit a straight line between three or more data points. In each case, the solid line shows experimental values and the segmented line shows theoretical predictions.

A careful inspection of the graphical results shows that certain trends are followed on DYNA3D predictions depending on initial kinetic energy of the projectile. On one hand, the ballistic limits predicted were consistently lower than the experimental ones at the lower areal densities. This was particularly observed in the case of the 44-grain fragment, where the analytical result lines for all areal densities were somewhat a parallel down shift of the experimental result lines. In the cases of 5.8- and 17-grain fragments the analytical results were either close or lower than the experimental results for the lower areal densities and higher for the higher areal densities, thus the analytical lines intersected the experimental lines. This finding would lead us to believe that the model does not account for energy absorbed due to certain failure modes observed in experiment. Extensive delamination, fiber pull-out and frictional dissipation of energy may be some of the failure and energy absorption mechanisms that the macromechanical model studied herein does not consider and thus underpredicts the experiment. This is particularly true in the cases where either a higher grain size projectile was used or a lower areal density wall was impacted. In these cases a lower kinetic energy and thus a lower velocity is required to penetrate the laminate and therefore the strain rates due to dynamic loading are not as severe as to reduce material properties substantially.

On the other hand, the ballistic limits predicted were substantially higher than the experimental ones when either higher areal densities or lower grain sizes were used. This was observed in the cases of the 17-grain fragment at the high end areal densities and of the 5.8-grain fragment in almost all areal densities. In these cases a higher kinetic energy, and therefore a higher initial velocity, is required. The energy absorption capability is a function of the impact velocity and therefore of the initial kinetic energy. However, increasing velocity in experiment induces higher fiber strains rates and therefore decreases material properties. DYNA3D does not have the capability of accounting for strength reduction due to high strain rates and therefore overpredicts the experiment.

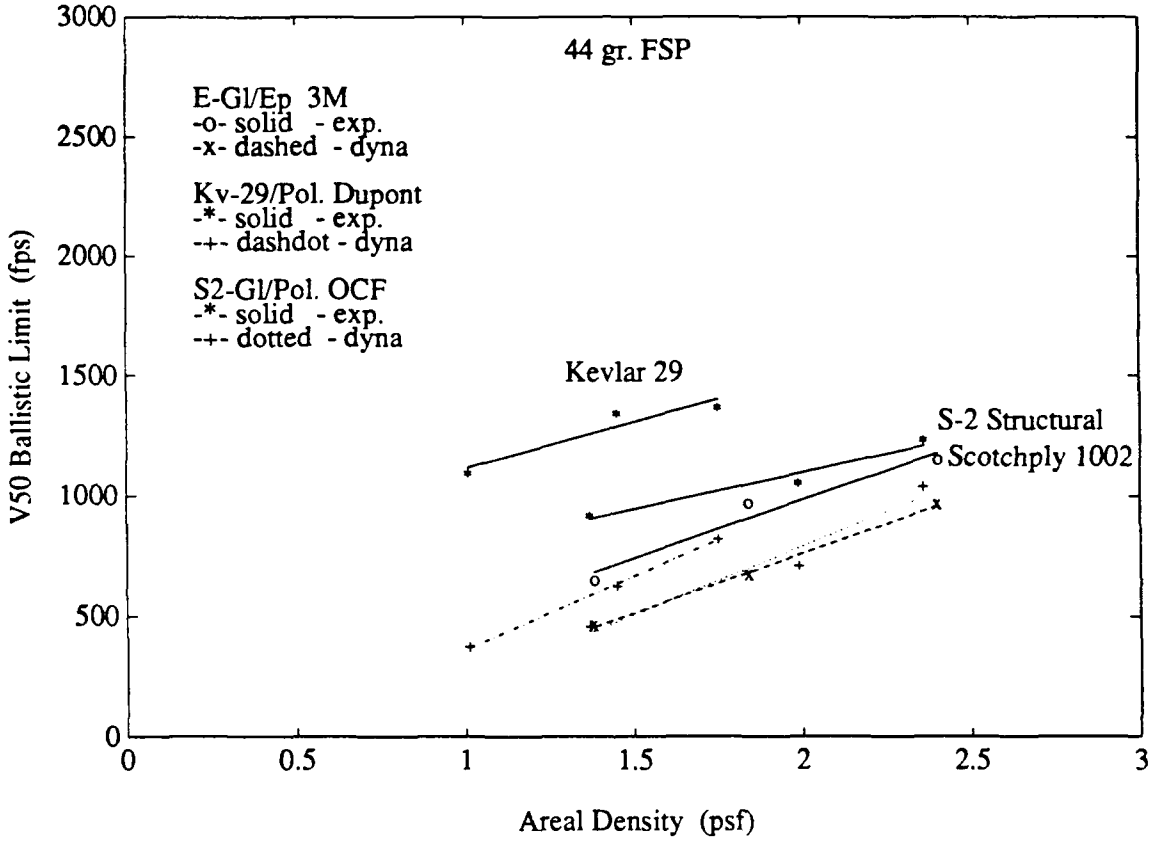

Figure 8. Graphical Comparison of DYNA3D to Experiment, 44-Grain FSP.

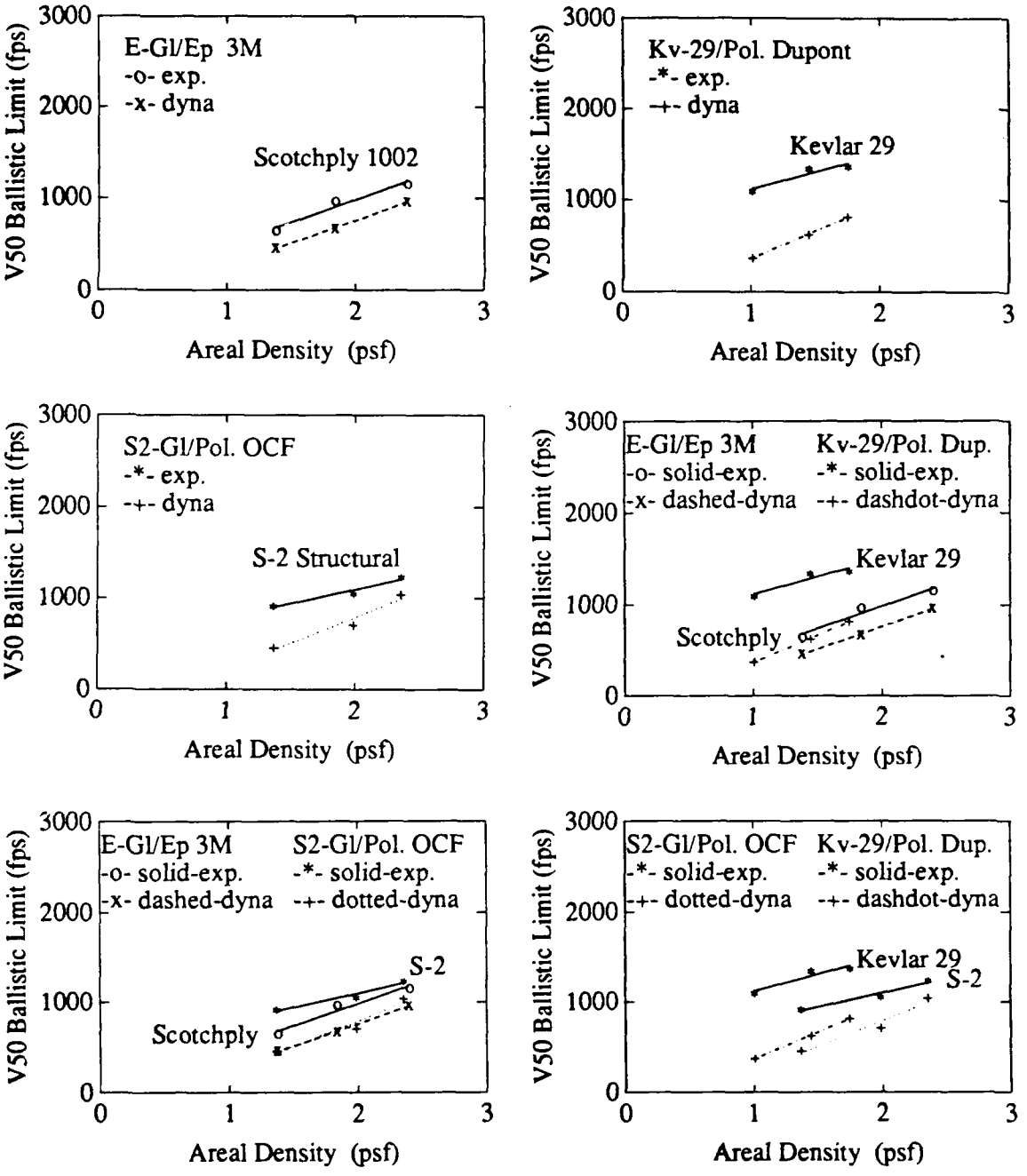

Figure 9. Individual and Pair Comparisons of DYNA3D to Experiment, 44-Grain FSP used, Materials used: Scotchply, S-2 Glass, Kevlar 29.

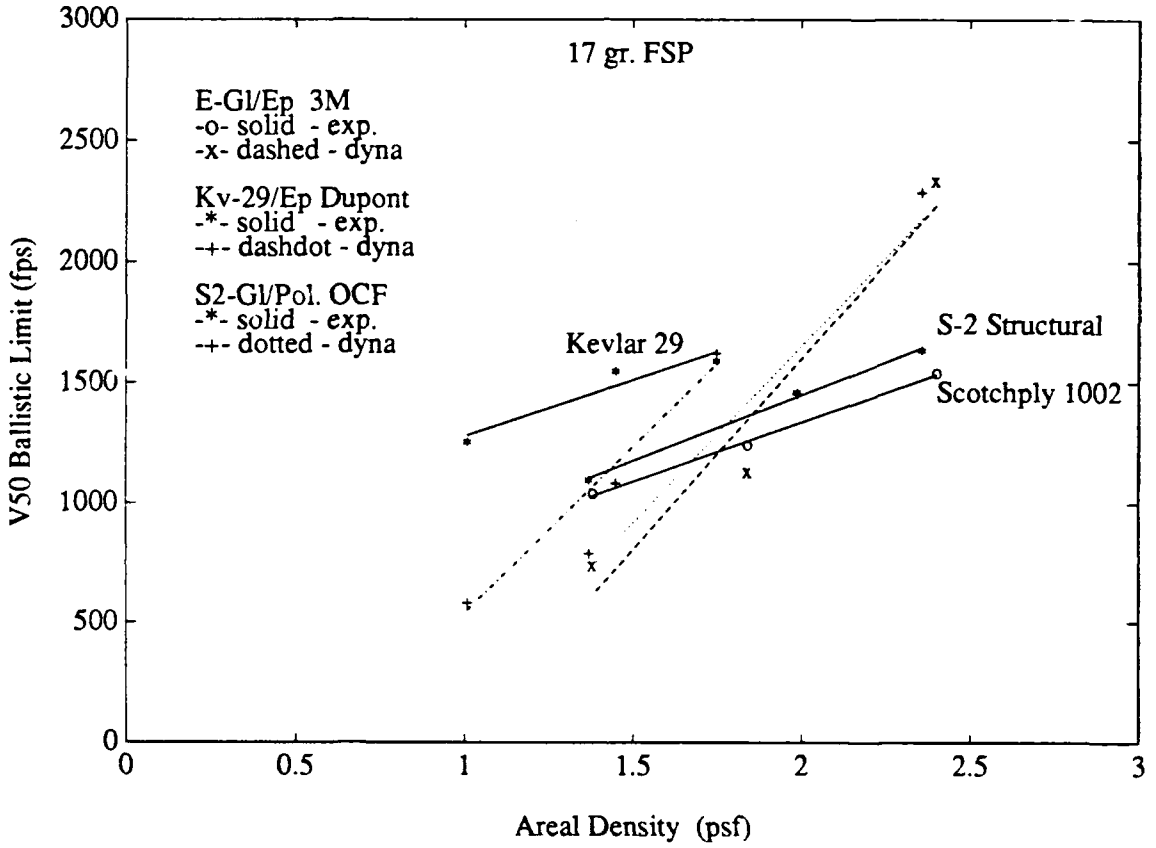

Figure 10. Graphical Comparison of DYNA3D to Experiment, 17-Grain FSP.

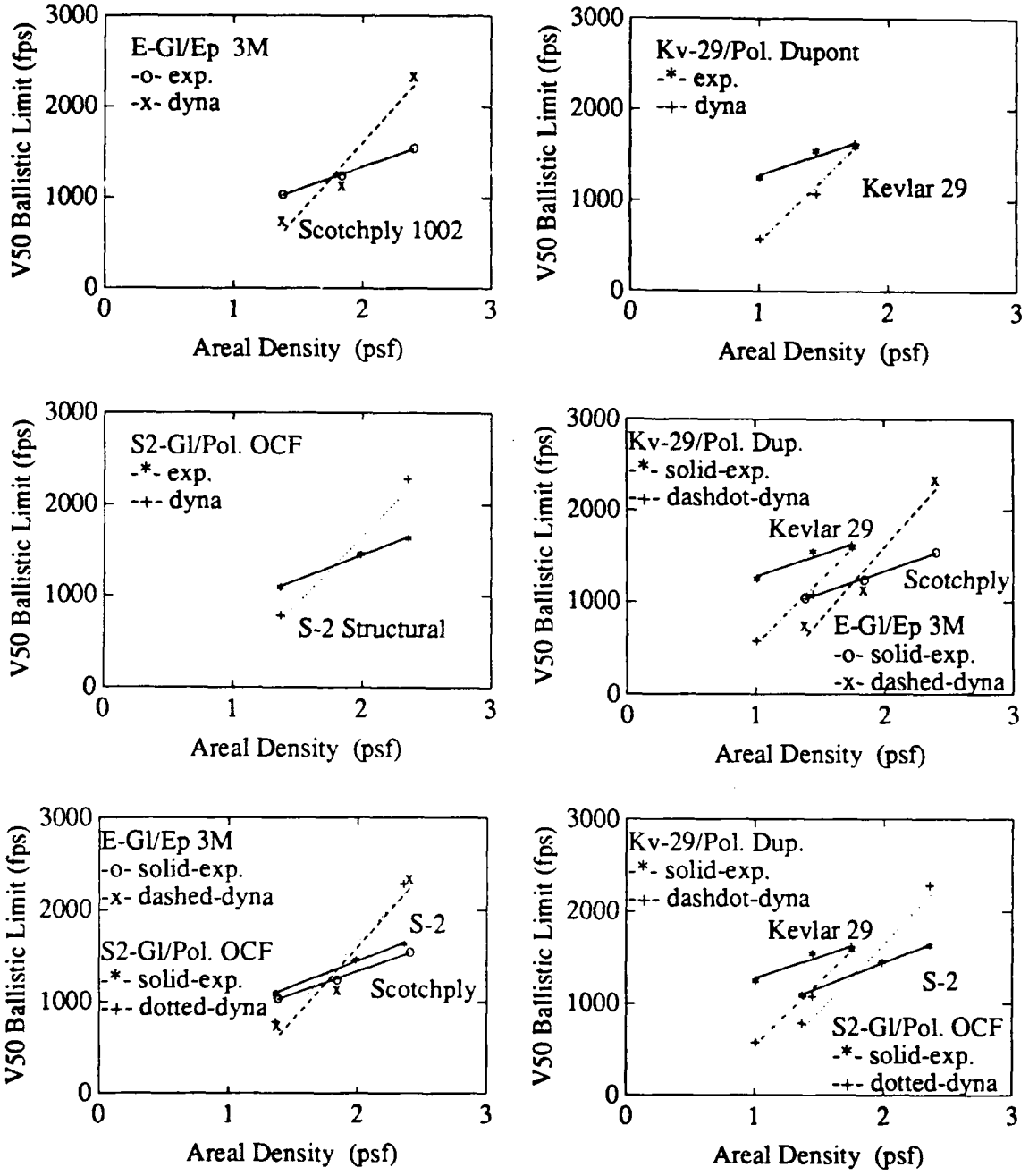

Figure 11. Individual and Pair Comparisons of DYNA3D to Experiment, 17-Grain FSP used, Materials used: Scotchply, S-2 Glass, Kevlar 29.

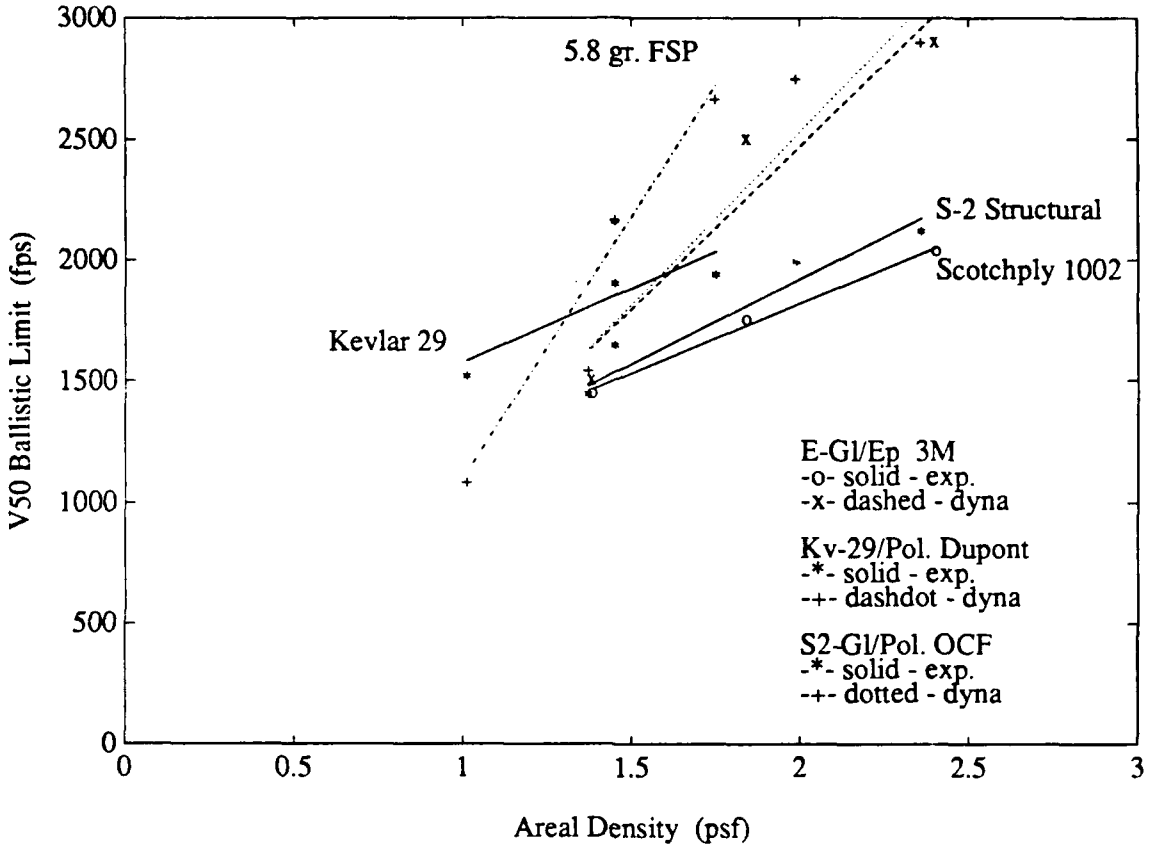

Figure 12. Graphical Comparison of DYNA3D to Experiment, 5.85-Grain FSP.

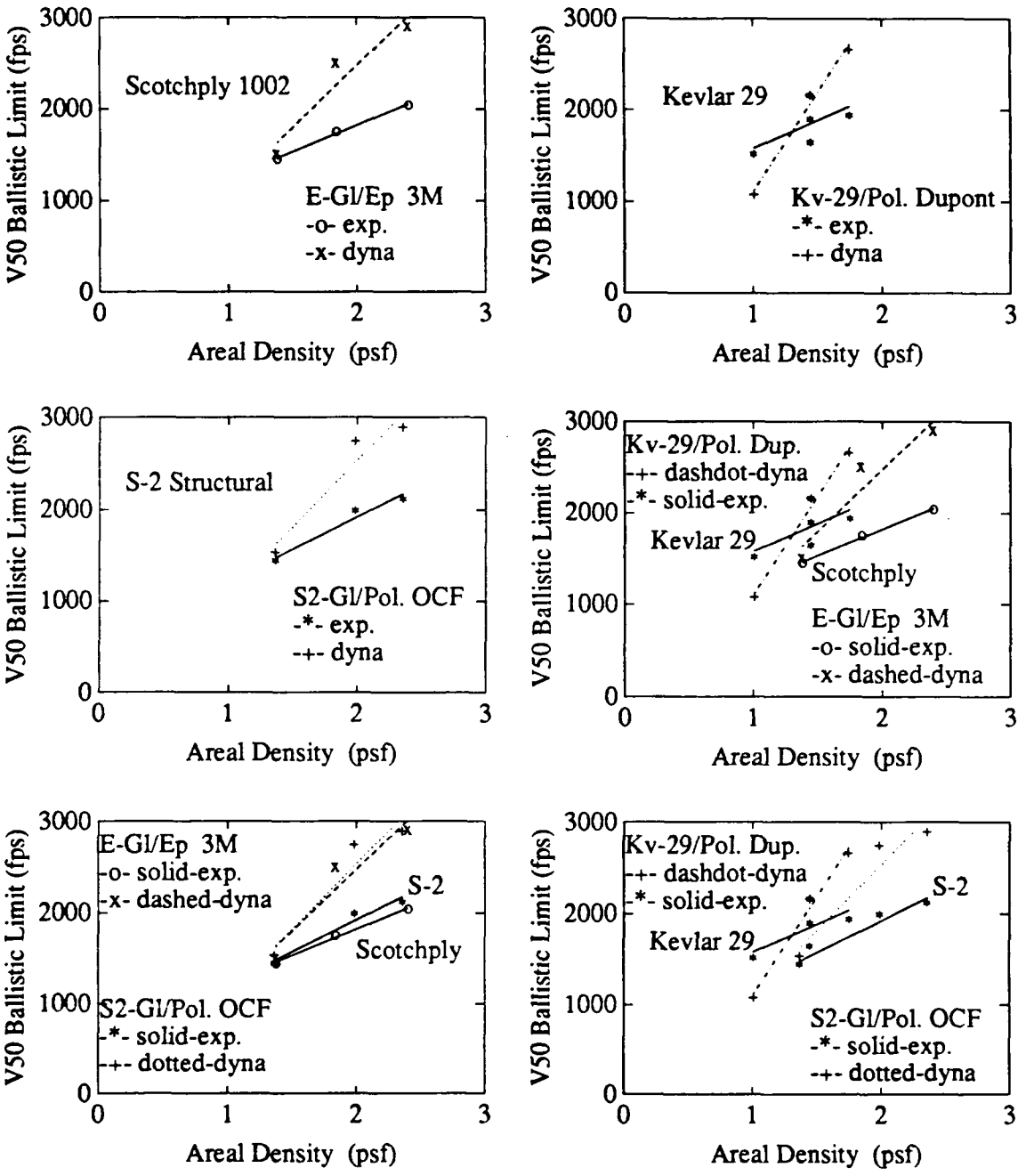

Figure 13. Individual and Pair Comparisons of DYNA3D to Experiment, 5.85-Grain FSP used, Materials used: Scotchply, S-2 Glass, Kevlar 29.

Parametric Studies

The effect of varying material properties on the ballistic limit was studied by conducting parametric studies. The three most critical properties affecting the resistance of the composite wall to fragment penetration are : Axial modulus Ex, Tensile Strength Xt, and Compressive strength Yc [Appendix A]. Here because of the orientation of the wall material (crossply or woven), the average material properties are the same in the x and y directions.

Table 5. Comparison of Ballistic Data Due to Property Change for a 0.2-inch thick S-2 Glass Structural Panel.

Properties Changed	Reduced by (%)	BALLISTIC LIMIT (V50) - (ft/sec)					
		17 Grains			44 Grains		
		Reduced	Initial	% diff.	Reduced	Initial	% diff.
Ex	30	1280	1458	12	650	710	8
Xt	30	1120	1458	23	580	710	18
Yc	30	1180	1458	19	585	710	17

Table 6. Comparison of Ballistic Data Due to Property Change for a 0.2-inch thick 3M Scotchply Wall.

Properties Changed	Reduced by (%)	BALLISTIC LIMIT (V50) - (ft/sec)					
		17 Grains			44 Grains		
		Reduced	Initial	% diff.	Reduced	Initial	% diff.
Ex	30	1000	1125	11	630	670	6
Xt	30	920	1125	18	600	670	10
Yc	30	950	1125	15	610	670	9

Table 7. Comparison of Ballistic Data Due to Property Change for a 0.2-inch thick Kevlar-29 Wall.

Properties Changed	Reduced by (%)	BALLISTIC LIMIT (V50) - (ft/sec)					
		17 Grains			44 Grains		
		Reduced	Initial	% diff.	Reduced	Initial	% diff.
Ex	30	985	1085	9	600	625	4
Xt	30	880	1085	19	550	625	12
Yc	30	900	1085	17	590	625	6

One of those three critical properties was changed while the other two were held constant in order to measure the net effect of each property on the ballistic limit. Critical properties were reduced by 30 percent in each case because the upper limit from the property variation was originally used. In addition, it would be expected that properties may be reduced due to environmental effects in the field. High strain rates of loading would also probably reduce the static properties used here. Results for a 0.2 inch thick wall are shown in Tables 5,6,7. Three different materials (S2 Glass, 3M Scotchply and Kevlar) and two different grain sizes (17, 44) were used.

Looking at the results it can be concluded that tensile properties control the ballistic penetration process. This is something that we would expect based on theoretical suggestions.

Conclusions and Recommendations

Conclusions

DYNA3D is a versatile finite element hydrocode, easily adopted and ported to any machine. Both pre and post processing capabilities are excellent. The code's structure allows the user to develop and add a new material model if necessary.

Based on results and comparisons to experiment, we conclude that DYNA3D's macromechanical model is a marginally acceptable analytical method of modeling penetration phenomena of composite laminates only if qualitative results are needed as a structural armor design criteria. However results should be carefully screened and experimentally verified if possible. High element distortions may create instabilities and error accumulations which could lead to either a non convergence of the solution or misleading results. In order to overcome this instability problem, rezoning is needed as distortions get large.

Depending on the initial kinetic energy of the projectile certain trends were followed by DYNA3D's predictions. The model predicts lower ballistic limits compared to experiment, in the cases where lower areal densities and higher projectile grain sizes were modeled and therefore lower initial kinetic energies were used. One possible explanation of this finding may be that the macromechanical model does not account for energy absorbed due to certain failure modes observed in experiment such as extensive delamination, fiber pull-out and frictional dissipation of energy, thus underpredicting the ballistic limit. On the other hand, the ballistic limit was overpredicted by DYNA3D when higher areal densities and/or lower projectile grain sizes were used which require higher initial kinetic energies. This may be due to the inability of the model to account for strength reduction due to high rates of loading and high rates of strain.

Parametric studies show that tensile properties of the composite panels control the ballistic penetration resistance by fragments. This is in contrary to the penetration process of metals where compressive properties and shear banding are dominant.

Of the three materials modeled, Kevlar-29 laminates were found to have the higher ballistic resistance as plotted versus areal density for each of the three fragment sizes used. Also of the two Glass materials modeled, S-2 glass Polyester laminates were found to have a slightly better ballistic performance than Scotchply.

Recommendations

Presently, there is a lack of knowledge of high strain rates properties of most composite materials. Further research is needed on the effects of high rates of loading and high strain rates on

dynamic properties of materials. A property degradation model, updating the local material properties of the damaged zone around the failed material as a function of strain rates is needed.

Furthermore, if quantitative and accurate results are desired, a new micromechanical material model needs to be considered. Development of such a micromechanical model requires knowledge of the actual failure modes observed during penetration and therefore an extensive study of fiber to matrix interaction during impact. Constitutive and failure equations need to be developed including high strain rates situations and their effects on the material properties and interaction of both fibers and resin. Stress wave propagation and deflection in heterogeneous media, such as the fiber-resin system, should also be addressed.

Here we should mention that the development of a micromechanical material model is an enormous task that would require many man-years of theoretical and experimental research efforts. Both analytical, computational methods and experimental techniques, such as dynamic characterization of materials and intense ballistic testing, are needed to better understand and consequently solve the penetration problem of composite materials.

This document reports research undertaken at the U.S. Army Natick Research, Development and Engineering Center and has been assigned No. NATICK/TR-92/019 in the series of reports approved for publication.

References

1. J. A. Zukas, T. Nicholas, H. F. Swift, L. B. Greszczuk, D. R. Curran, "Impact Dynamics," John Wiley and Sons, Inc., 1982.

2. F. C. Hodi, "Ballistic Evaluation of Glass-Reinforced Plastic, Kevlar-29 Laminates, and Shelter Wall Combinations," Materials Dynamics Branch, U.S. Army MTL, Watertown, MA., MTL TR 89-60, Sponsored by ETD/AMED, U.S. Army Natick RD&E Center, Natick, MA., July, 1989.

3A. J. O. Hallquist, "DYNA3D User's Manual," LLNL, CA., Rev. April 1988.
3B. J. O. Hallquist, "DYNA3D Course Notes," LLNL, CA., UCID 19899, Rev. 2, November, 1987.
3C. J. O. Hallquist, "Theoretical Manual for DYNA3D," LLNL, CA., UCID 19401, March, 1983.

4. J. Little, C. Moler, S. Bangert, "MATLAB Interactive Scientific and Engineering Software - 2D Graphics," The Mathworks, Inc., Sherborn, MA., 1987.

5. R. M. Jones, "Mechanics of Composite Materials," Scripta Book Co., Washington, D.C., 1975.

6. S. J. Bless, R. V. Krolak, D. R. Askins, "Evaluation of Lightweight Materials for Shelter Armors," University of Dayton, Dayton, Ohio, Prepared for ETD/AMED, U.S. Army Natick RD&E Center, Natick, MA., Natick/TR-86/046L, July, 1986.

7. F. K. Chang and K. Y. Chang, "A Progressive Damage Model for Laminated Composites Containing Stress Concentration" and "Post-Failure Analysis of Bolted Composite Joints in Tension or Shear-Out Mode Failure," Journal of Composite Materials, Volume 21, pp. 809-855, 1987.

8. D. W. Stillman and J. O. Hallquist, "INGRID: A 3D Mesh Generator for Modeling Nonlinear Systems," LLNL, CA., UCID 20506, Rev. July, 1985.

9. B. E. Brown and J. O. Hallquist, "TAURUS: An Interactive Post-Processor for the Analysis Codes NIKE3D, DYNA3D, TACO3D, and GEMINI," LLNL, CA., UCID 19392, Rev. 1, May, 1984.

10. A. M. Blanas, "Analytical Modeling of Fragment Penetration of Composite Shelter Laminates," Proceedings of the 3rd Natick Science Symposium, U.S. Army RD&E Center, Natick, MA., June 5-6, 1990.

11. D. R. Hartman, "Typical Properties for OCF S-2 Glass/Polyester Laminates," Fax Transmittal, Owens Corning Fiberglass, Granville, Ohio, March 1991.

12. "Properties of Scotchply Reinforced Plastics," Structural Products Department, 3M, St. Paul, MN., June 1985.

13. "A Guide to Designing and Preparing Ballistic Protection of Kevlar(R) Aramid," Du Pont Company, Textile Fibers Department, Wilmington, Delaware, January 1983.

14. S. W. Tsai and H. T. Hahn, "Introduction to Composite Materials," Technomic Publishing Co., Inc., Westport, CT., 1980.

15. S. W. Tsai, T. N. Massard, I. Susuki, "Composites Design," 4th Ed., Think Composites, Dayton, Ohio, 1988.

APPENDIX A

Properties of Materials Used

Appendix A

Properties of Materials Used

Three materials were used for modeling purposes. Their properties are reported here.

Table A-1. Typical Material Properties of Laminates Used.

PROPERTY	OCF S2-Glass Structural Woven [11]	3M E-Glass Scotchply X-Ply [12]	Du Pont Kv29/Pol Woven [13]
Elastic Constants	**10^6 PSI**	**10^6 PSI**	**10^6 PSI**
Longitudinal Modulus, Ex	4.6	3.5	4.1
Transverse Modulus, Ey	4.6	3.5	4.1
Z-Direction Modulus, Ez	1.7	1.4	0.8
Shear Modulus, Gxy	1.1	0.7	0.4
Poisson's Ratio, ν_{xy} (for unidirectional)	0.25	0.25	0.34
Strength Properties	**10^3 PSI**	**10^3 PSI**	**10^3 PSI**
Longitudinal Tension, X	120.0	70.0	70.0
Transverse Tension, Y	120.0	70.0	70.0
Longitudinal Compression, X'	80.0	60.0	40.0
Transverse Compression, Y'	80.0	60.0	40.0
In-Plane Shear, S	11.0	11.0	3.0
X-Ply Shear, based on Laminate Thickness, Sc	11.0	9.0	5.0
Physical Properties			
Fiber Volume (%)	65.0	64.0	65.0
Density (lb/in^3), ρ	0.075	0.065	0.052
Ply Thickness (in)	0.02	0.01	0.02

Table A-2. Properties of Steel Fragment Simulating Projectiles.

Property		
Young's Modulus, E	30.0	10^6 PSI
Poisson's Ratio, ν	0.3	
Yield Stress, σ_{ys}	150.0	10^3 PSI
Hardening Modulus, E_t	10.0	10^4 PSI
Density, ρ	0.28	lbs/in^3

APPENDIX B

Sample Input Files for DYNA3D

Appendix B

Sample Input Files for DYNA3D

Three sample input files are shown here. These input files are actually inputed to the pre-processor INGRID which generates the model's geometry mesh, material description and initial conditions. The output file of the pre-processor, a quite large file in size, is then used as an input file to DYNA3D.

The three INGRID's input files are listed in Table B-1. Commends have been added to the files for easy reading.

Table B-1. Input Files for INGRID.

File	Material	Areal Density (psf)	Fragment Size (Grains)
FILE 1	3M E-Gl/Ep.	1.38	5.85
FILE 2	OCF S2-Gl/Pol.	1.99	17.0
FILE 3	DUP. Kv29/Pol.	1.75	44.0

FILE 1

```
3MSchp 1/2 sym. 5.8grn .15"                {E-Glass/Epoxy x-ply}
dn3d                                       {areal density 1.38 psf}

c fragment inner part lines                { definition of 5.85 gr fragment}
ld 30 lp 2 .001 0 .001 .18                  { lines 30,31,32,33 }
ld 31 lp 2 .001 .18 .0751 .18
ld 32 lp 2 .001 0 .0751 0
ld 33 lp 2 .0751 0 .0751 .18

si 1 tied;si 2 sv;si 3 tied;               {definition of slide surfaces}
plane 1 0 0 0 0 1 0 .001 symm              { plane of half symmetry }
term 1.3e-4  prti  .1 plti 1.e-6           { set time of total run and }


mat 1 3 head                               { definition of material 1 type 3
steel fragment projectile                  { steel fragment properties}
ro 7.?02e-4 e 3.e7 pr .3
sigy 150.e3 etan 1.2e5
```

```
mat 2 22 head                                   {definition of material 2 type 22}
glass/ep  orthotropic comp damage x-ply
ro 1.7e-4 ea .357e7 eb .357e7 ec .14e7
c  kf .1e7
prba .1 prca .14 prcb .14
gab .07e7 gbc .07e7 gca .07e7
aopt 0 xt 70e3 yt 70e3
yc 60e3  sc 9e3
endmat

c fragment inner part                           {part definition}
part 32 33 31 30 1 4 4                          {5.85 gr fragment}
drag rota 6 0 0 0 0 0 1 180;
si 1 1 1 2 2 1 2 m { bottom s.v.}
si 2 1 1 2 2 2 2 m { side s.v. }
c b 1 2 1 2 2 2  010111 {y symmetry}
velo 0 0 -18000.                                { initial projectile velocity}
end

c wall inner part                               { wall inner fine mesh part}
start
1  14;1 7 ;1 6;
-.15  .15  0 -.15 0 -.15
mate 2                                          {definition of slide surfaces}
 si 2 1 1 2 2 2 1 s                             {side outter tied slave x-plane}
 si 1 1 1 1 2 2 1 s                             {side outter tied slave x-plane}
 si 1 2 1 2 2 2 1 s                             {side outter tied slave y-plane}
 si 1 1 1 2 2 1 2 s                             {top s.v. slave for inner frg }
end

c wall outer part                               { wall outer coarse mesh}
start
1 3 7 14 18 20; 1 5 8 11 ; 1 6;
-.76 -.38 -.15 .15 .38 .76 0 -.15 -.38 -.76 0 -.15
mate 2
di 0 0 3 4 0 0;1 2 0 0;1 2;
c si 1 1 2 2 2 2 3 m                            {definition of sliding interfaces
si 3 2 1 4 2 2 1 m                              {side inner tied master y-plane}
si 4 1 1 4 2 2 1 m                              {side inner tied master x-plane}
si 3 1 1 3 2 2 1 m                              {side inner tied master x-plane}

b  1 1 1 1 4 2 111111 {x-plane fixed}
b  6 1 1 6 4 2 111111 {x-plane fixed}
b  1 4 1 6 4 2 111111 {y-plane fixed}
c b  1 1 1 6 1 2 010111 {symmetry y}
end
end
```

FILE 2

```
S2/ep 1/2 sym. 17grn .2"                    {S2-Glass polyester woven laminate}
dn3d                                        {areal density 1.99 psf}

c fragment outer part lines                 {definition of 17 grain fragment}
ld 3 lp 2 .051 0 .051 .27                   { lines 3,4,5,14 outer part}
ld 4 lp 2 .051 0 .107 .082
ld 5 lp 2 .107 .082 .107 .27
ld 14 lp 2 .051 .27 .107 .27

c fragment inner part lines                 { definition of 17 gr fragment}
ld 30 lp 2 .001 0 .001 .27                  {lines 30,31,32,33 inner part}
ld 31 lp 2 .001 .27 .051 .27
ld 32 lp 2 .001 0 .051 0
ld 33 lp 2 .051 0 .051 .27

si 1 tied;si 2 sv;si 3 tied;                {definition of sliding interfaces}
plane 1 0 0 0 0 1 0 .001 symm               { plane of symmetry}
term 1.2e-4  prti  .1 plti 1.e-6            {total time and time of result states}

mat 1 3 head                                {definition of material 1 type 3}
steel fragment projectile                   { fragment properties}
ro 7.202e-4 e 3.e7 pr .3
sigy 150.e3 etan 1.0e5

mat 2 22 head                               {definition of material 2 type 22}
S2 glass/ep orthotropic comp damage x-ply
ro 2.02e-4 ea .46e7 eb .46e7 ec .17e7
c  kf .1e7
prba .103 prca .144 prcb .144
gab .11e7 gbc .11e7 gca .11e7
aopt 0 xt 120e3 yt 120e3
yc 80e3  sc 11e3
endmat

                                            {part definition}
c fragment outer part
part 4 5 14 3 1 2 4                         {outer fragment}
drag rota 6 0 0 0 0 0 1 180;
 si 2 1 1 2 2 2 2 m {side s.v}              {sliding interfaces}
 si 1 1 1 1 2 2 3 m {side tied}
 si 1 1 1 2 2 1 2 m {bottom s.v}
velo 0 0 -17500.                            {initial projectile velocity}
end

c fragment inner part                       {inner projectile part}
part 32 33 31 30 1 2 4
drag rota 6 0 0 0 0 0 1 180;
si 1 1 1 2 2 1 2 m { bottom s.v.}
 si 2 1 1 2 2 2 3 s {side tied}
velo 0 0 -17000.                            {initial velocity}
end
```

```
c wall inner part                                    {wall inner fine mesh}
start
1  14;1 7 ;1 6;
-.15  .15  0 -.15 0 -.2
mate 2                                               {definition of sliding surfaces}
 si 2 1 1 2 2 2 1 s                                  {side outter tied slave x-plane}
 si 1 1 1 1 2 2 1 s                                  {side outter tied slave x-plane}
 si 1 2 1 2 2 2 1 s                                  {side outter tied slave y-plane}
 si 1 1 1 2 2 1 2 s                                  {top s.v. slave for inner frg }
end

c wall outer part                                    {wall outer coarse mesh}
start
1 3 7 14 18 20; 1 5 8 11 ; 1 6;
-.76 -.38 -.15 .15 .38 .76 0 -.15 -.38 -.76 0 -.2


 mate 2
 di 0 0 3 4 0 0;1 2 0 0;1 2;
 c si 1 1 2 2 2 2 3 m                                {sliding surfaces}
 si 3 2 1 4 2 2 1 m                                  {side inner tied master y-plane}
 si 4 1 1 4 2 2 1 m                                  {side inner tied master x-plane}
 si 3 1 1 3 2 2 1 m                                  {side inner tied master x-plane}
                                                     {fixed boundaries}
 b  1 1 1 1 4 2 111111 {x-plane fixed}
 b  6 1 1 6 4 2 111111 {x-plane fixed}
 b  1 4 1 6 4 2 111111 {y-plane fixed}
 end
 end
```

FILE 3

```
kevlar 1/2 sym. 44grn .24"          {kv-29/pol. woven laminate }
dn3d                                {areal density 1.75 psf }

c fragment outer part lines         { definition of the fragment }
ld 3 lp 2 .071 0 .071 .38           { lines, 3,4,5,14, outer part}
ld 4 lp 2 .071 0 .151 .05
ld 5 lp 2 .151 .05 .151 .38
ld 14 lp 2 .071 .38 .151 .38

c fragment inner part lines         { definition of the fragment }
ld 30 lp 2 .001 0 .001 .38          { lines 30,31,32,33 inner part}
ld 31 lp 2 .001 .38 .071 .38
ld 32 lp 2 .001 0 .071 0
ld 33 lp 2 .071 0 .071 .38

si 1 tied;si 2 sv;si 3 tied;        { definition of sliding interfaces}
plane 1 0 0 0 0 1 0 .001 symm       { plane of half symmetry}
term 1.3e-4  prti  .1 plti 1.e-6    { set time of total run and time of}
                                    { plotting states}
mat 1 3 head
steel fragment projectile           { definition of material 1 type 3 }
ro 7.202e-4 e 3.e7 pr .3 sigy       { steel fragment properties}
150.e3 etan 1.0e5

mat 2 22 head                       { definition of material 2 type 22}
kevlar 29 comp damage crossply
ro 1.4e-4 ea .41e7 eb .41e7
ec .08e7 {kf .1e7}
prba .05 prca .07 prcb .07
gab .04e7 gbc .04e7 gca .04e7
aopt 0 xt 70e3 yt 70e3
yc 40e3  sc 5e3
endmat

                                    { part definitions}
c fragment outer part               { outer fragment part}
part 4 5 14 3 1 2 4
drag rota 6 0 0 0 0 0 1 180;
 si 2 1 1 2 2 2 2 m {side s.v}      {sliding interfaces for part}
 si 1 1 1 1 2 2 3 m {side tied}
 si 1 1 1 2 2 1 2 m {bottom s.v}
velo 0 0 -9850.                     {projectile initial velocity}
end
c fragment inner part               { inner fragment part }
part 32 33 31 30 1 2 4
drag rota 6 0 0 0 0 0 1 180;
si 1 1 1 2 2 1 2 m { bottom s.v.}
 si 2 1 1 2 2 2 3 s {side tied}
velo 0 0 -9850.                     {initial projectile velocity}
end
```

```
c wall inner part                          { wall inner fine mesh part}
start
1  14;1 7 ;1 6;
-.15  .15  0 -.15 0 -.24
mate 2                                      {definition of slide surfaces}
 si 2 1 1 2 2 2 1 s                         {side outter tied slave x-plane}
 si 1 1 1 1 2 2 1 s                         {side outter tied slave x-plane}
 si 1 2 1 2 2 2 1 s                         {side outter tied slave y-plane}
 si 1 1 1 2 2 1 2 s                         {top s.v. slave for inner frg }
end
c wall outer part                          {wall outer coarse mesh}
start
1 3 7 14 18 20; 1 5 8 11 ; 1 6;
-.76 -.38 -.15 .15 .38 .76 0 -.15 -.38 -.76 0 -.24
mate 2
di 0 0 3 4 0 0;1 2 0 0;1 2;


c si 1 1 2 2 2 2 3 m                         {definition of sliding interfaces}
si 3 2 1 4 2 2 1 m                           {side inner tied master y-plane}
si 4 1 1 4 2 2 1 m                           {side inner tied master x-plane}
si 3 1 1 3 2 2 1 m                           {side inner tied master x-plane}

b  1 1 1 1 4 2 111111 {x-plane fixed}   { outer boundary conditions fixed}
b  6 1 1 6 4 2 111111 {x-plane fixed}
b  1 4 1 6 4 2 111111 {y-plane fixed}
end
end
```

APPENDIX C

Calculations

Appendix C

Calculations

Kinetic Energy Check

Hand calculations checking the Kinetic Energy calculations of DYNA3D were performed. A sample hand calculation for the case of 3M Scotchply Glass, areal density 1.38 (psf), impacted by a 5.85 grain steel fragment, is shown below. Input file for this case is listed as FILE 1 in Appendix B.

Initial Velocity of Fragment V = 18,000.00 in/sec.

Mass of Fragment $M = (5.85 \text{ grain}) \times (1\text{b} / 7000 \text{ grain}) \times (1 / 386 \text{ in/sec}^2)$

or $M = 2.165 \times 10^{-6} (1\text{b} - \text{sec}^2) / \text{in}$

Kinetic Energy Hand Calculation

$$KEh = 1/2 \times M \times V^2$$

or $$KEh = 1/2 \times 2.165 \times 10^{-6} [(1\text{b} - \text{sec}^2) / \text{in}] \times 18000^2 (\text{in}^2 / \text{sec}^2)$$

or $$KEh = 351 \text{ in} - \text{lbs}$$

Since half symmetry is used for the model, the Kinetic Energy is

$$KEh \text{ hand} = 175.5 \text{ in} - \text{lbs}$$

Kinetic Energy as Calculated by DYNA3D for the model is

$$KEd \text{ dyna} = 177.5 \text{ in} - \text{lbs}$$

The hand calculation checks within 1.1 % of the model's calculation of Kinetic Energy.

In some cases, when the more geometrically complicated 17 or 44 grain fragments were modeled, the DYNA3D calculation of Kinetic Energy was within 5 % lower of the hand calculated one. This is due to the approximate nature of the finite element modeling and the rather coarse mesh used for the fragment model. If a finer geometric mesh is used the difference dramatically improves. In addition, even though the same dimensions were used for the model as outlined in FSP, MIL-P-46593A, some mass differences may result from slightly different mass densities used for the steel fragment.

Properties Calculation

Sample calculations of some elastic constants and properties that were not experimentally available are shown here for 3M Scotchply glass. Similar calculations were used to predict some properties for S2 glass and Kevlar 29. Woven composites were replaced by a [0/90] laminate of the same thickness as proposed by [14], [15]. This replacement approach has been proven to give accurate predictions.

Density

For 3M Scotchply $\rho = 0.065$ lb/in^3. Divide by g = 386 in/sec^2, to convert density to units compatible to the code.

$$\rho_{3M} = (0.065 \text{ lb/in}^3) / (386 \text{ in/sec}^2)$$

or

$$\rho_{3M} = 1.68 \times 10^{-4} [(\text{lb} - \text{sec}^2) / \text{in}^4]$$

Poisson's Ratio and Shear Modulus

The following properties of a unidirectional ply with coordinate system shown in Figure 14, were used as input into laminate plate theory code "Genlam" [15].

Ex = 5.7 Msi, Ey = 1.4 Msi, Es = .7 Msi, $\nu_{xy} = .25$.

A symmetric [0/90]s cross-ply laminate is considered here. The output of "Genlam" gives the following calculated properties for the x-ply laminate.

Ex [0/90] = 3.5 Msi, Ey [0/90] = 3.5 Msi, Es [0/90] = .7 Msi,

ν_{xy} [0/90] = ν_{yx} [0/90] = 0.10

The Poisson's ratio's used in the model were derived as follows.

Assumptions

Unidirectional	X - Ply
$\nu_{yz} = 1.8\ \nu_{xy}$	$\nu_{xz} = \nu_{yz} = (\nu_{xz\ uni} + \nu_{yz\ uni}) / 2$
$\nu_{xz} = \nu_{xy} = .25$	Ez x-p = Ey uni = .14e7 Psi
	Gxy = Gyz = Gzx = .07e7 Psi.

Based on the above assumptions we calculate,

$$\nu_{xz\ x\text{-}ply} = \nu_{yz\ x\text{-}ply} = (\nu_{xy\ uni} + 1.8\ \nu_{xy\ uni}) / 2$$

$= 1.4\ \nu_{xy\ uni} = 0.35$

therefore for the X - Ply we calculate,

$$(\nu_{xz\ x\text{-}p} / Ex\ x\text{-}p) = (\nu_{zx\ x\text{-}p} / Ez\ x\text{-}p)$$

$$(.35 / .35e7) = (\nu_{zx\ x\text{-}p} / .14e7)$$

$$\nu_{zx\ x\text{-}p} = 0.14$$

similarly $\nu_{zy\ x\text{-}p} = 0.14$

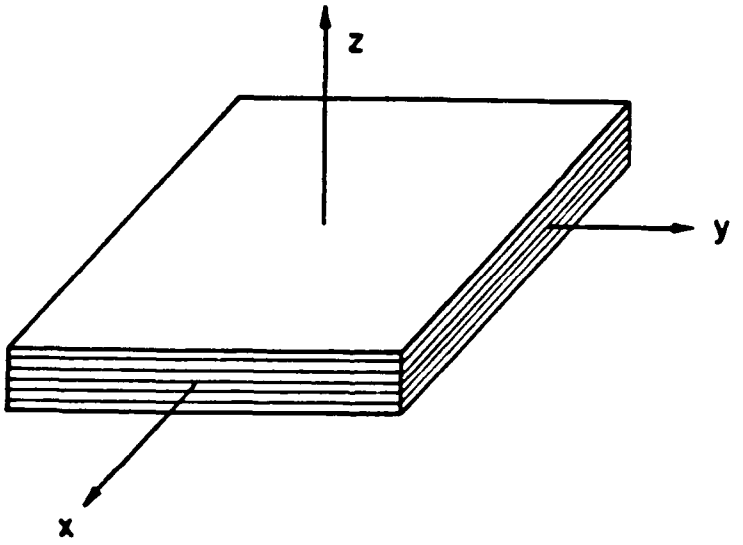

Figure 14. Coordinate System for a Unidirectional Lamina, X is Fiber Direction. X-ply Laminate has the Same Geometric Directions.